

The DEEP Groth Strip Survey VI. Spectroscopic, Variability, and X-ray Detection of AGN

Vicki L. Sarajedini

University of Florida, Department of Astronomy, Gainesville, FL 32611; vicki@astro.ufl.edu

David C. Koo¹, Andrew C. Phillips¹, Henry A. Kobulnicky², Karl Gebhardt³, Christopher N. A. Willmer¹, Nicole P. Vogt⁴, Elise Laird⁵, Myungshin Im⁶, Sarah Iverson⁷, and Wanessa Mattos⁸

ABSTRACT

We identify active galactic nuclei (AGN) in the Groth-Westphal Survey Strip (GSS) using the independent and complementary selection techniques of optical spectroscopy and photometric variability. We discuss the X-ray properties of these AGN using Chandra/XMM data for this region. From a sample of 576 galaxies with high quality spectra we identify 31 galaxies with AGN signatures. Seven of these have broad emission lines (Type 1 AGNs). We also identify 26 galaxies displaying nuclear variability in HST WFPC2 images of the GSS separated by ~ 7 years. The primary overlap of the two selected AGN samples is the set of broad-line AGNs, of which 80% appear as variable. Only a few narrow-line AGNs approach the variability threshold. The broad-line AGNs have an average redshift of $\langle z \rangle \simeq 1.1$ while the other spectroscopic AGNs have redshifts closer to the mean of the general galaxy population ($\langle z \rangle \simeq 0.7$). Eighty percent of the identified broad-line AGNs are detected in X-rays and these are among the most luminous X-ray sources in the GSS. Only one narrow-line AGN is X-ray detected. Of the variable nuclei galaxies within the X-ray survey, 27% are X-ray detected. We find that $1.9 \pm 0.6\%$ of GSS galaxies to $V_{gal}=24$ are broad-line AGNs, $1.4 \pm 0.5\%$ are narrow-line AGNs, and $4.5 \pm 1.4\%$ contain variable nuclei. The fraction of spectroscopically identified BLAGNs and NLAGNs at $z \sim 1$ reveals a marginally significant increase of $1.3 \pm 0.9\%$ when compared to the local population.

Subject headings: galaxies:active–surveys

1. INTRODUCTION

Active galaxies, galaxies accreting significant material onto a central supermassive blackhole, are some of the most intriguing objects in the universe. The first active galaxies were identified based on their extreme luminosities, emission line properties and ability to vary in luminosity over short time periods. Since then, several selection techniques have been employed to identify and study the active galaxy population. However, these techniques also imposed redshift limits on the selected samples. Quasars, the most luminous class of active galactic nuclei (AGN), can be iden-

¹UCO/Lick Observatory, University of California, Santa Cruz, CA 95064

²University of Wyoming, Department of Physics and Astronomy, Laramie, WY 82071

³University of Texas, Department of Astronomy, Austin, TX 78723

⁴New Mexico State University, Department of Astronomy, Las Cruces, NM 88003

⁵Astrophysics Group, Imperial College London, London, SW7 2AZ, UK

⁶Astronomy Program, SEES, Seoul National University, Seoul, Korea

⁷University of Iowa, Department of Physics and Astronomy, Iowa City, IA 52242

⁸University of Florida, Gainesville, FL 32611

tified out to high redshifts using most selection techniques, while the intrinsically fainter AGNs (e.g. Seyfert galaxies) are mostly limited to local samples.

This has led to a prominent gap in our current understanding of the AGN phenomenon; the connection between bright QSOs which exist in large numbers at redshifts of $z \simeq 2-3$ and low-luminosity Seyferts which have historically been studied at much lower redshifts. Understanding how the population of faint AGNs evolves with redshift is of particular importance for determining the frequency and total space density of AGNs at earlier epochs. This has obvious implications for determining their total contribution to the X-ray, IR and UV backgrounds. Large numbers of low-luminosity AGNs have been proposed to explain the ionization of the intergalactic medium at high redshift (Steidel & Sargent 1989), although recent observational and theoretical results differ on the amount of their true contribution (Barger *et al.* 2003a; Schirber & Bullock 2003). Additionally, the faint end of the AGN luminosity function (LF) is an important constraint on evolutionary models such as pure luminosity and luminosity-dependent density evolution (e.g. Boyle *et al.* 2000).

The AGN luminosity function has been well studied out to high redshifts for QSOs (e.g. Hartwick & Schade 1990) and several works measure the local luminosity functions for Seyfert galaxies (Cheng *et al.* 1985; Huchra & Burg 1992; Koehler *et al.* 1997; Ulvestad & Ho 2001; Londish *et al.* 2000; Maia *et al.* 2003; Hao *et al.* 2005). Most Seyfert LFs have been based on optical spectroscopically selected nuclei. However, spectroscopically selected samples of AGNs at high redshift are harder to obtain due to the inevitably lower signal-to-noise spectra, combined with the lack of suitable diagnostic emission lines in the optical portion of the spectrum that allow identifying AGNs.

Another identifying characteristic of active galaxies is their variability. QSOs and Seyfert galaxies have long been known as variable objects, with significant optical flux changes occurring on timescales of months to several years. While variability has been primarily used to identify QSOs (Hawkins 1986; Koo *et al.* 1986; Hook *et al.* 1994), Seyfert 1 galaxies have also been shown to vary

in broad-band photometric surveys (e.g. Peterson *et al.* 1998). A survey for variable sources in SA57 revealed many optically extended, Seyfert-like galaxies (Bershady *et al.* 1998) which generally had higher variability amplitudes than the more luminous QSOs. This result suggests that variability is a good technique for selecting intrinsically faint QSOs and Seyfert nuclei.

The purpose of this study is to employ two independent and complementary selection techniques to identify Seyfert-luminosity AGNs to redshifts of $z \sim 1$. We analyze the Deep Extragalactic Evolutionary Probe (DEEP) spectroscopic survey data of the Groth-Westphal Survey Strip (GSS; Groth *et al.* 1994) to detect and measure emission lines to determine the ionizing source within the galaxy and thus probe the population of active galaxies to $z \sim 1$. We further select candidate AGNs based on nuclear variability. Three-quarters of the GSS was re-imaged with HST ~ 7 years after the original WFPC2 images were obtained. We identify galaxies whose nuclei have significantly varied over this time interval in order to select potential active galaxies.

Thus, we compare/contrast the types of AGN identified using these two established optical selection techniques. In addition, we investigate how the AGN identified via optical selection manifest themselves in deep X-ray surveys of the GSS. This work constitutes the first comparison of these three AGN selection techniques for $z \sim 1$ galaxies and provides an important benchmark for future studies of AGN in deep surveys.

We describe the spectroscopic observations and line measurements in §2. In §3, we discuss the HST photometric survey and the identified variable galaxies. The selected AGN/AGN candidates are discussed and compared to typical GSS galaxies in §4 and §5. In §6, the X-ray sources in the GSS are discussed and compared to the results of the spectroscopic and variability surveys. We compute the relative fraction of Type 1 and 2 AGNs in §7 and summarize the results in §8.

2. THE SPECTROSCOPIC SURVEY

The Deep Extragalactic Evolutionary Probe (DEEP; Koo *et al.* 1996; Simard *et al.* 2002; Vogt *et al.* 2005; Weiner *et al.* 2005) is a galaxy redshift survey designed to study the formation and

evolution of distant field galaxies and large scale structure to $z \sim 1$. This paper uses the first phase of DEEP (DEEP1) which was carried out using the Low-Resolution Imaging Spectrometer (LRIS; Oke *et al.* 1994) on the Keck telescopes. The second phase of DEEP (DEEP2; Davis *et al.* 2003) is currently under way and uses the DEIMOS spectrograph (Faber *et al.* 2005) on the Keck 2 telescope. The Groth Survey Strip is one of the fields targeted by DEEP for spectroscopic observations and comprises 28 contiguous WFPC2 fields located at 14h17m+52, imaged in the V(F606W) and I(F814W) filters. The fields are numbered 4 through 31 diagonally across the sky. The GSS object IDs used throughout this paper indicate the GSS field (first 2 digits) and the Wide Field CCD number (third digit) in which each object was identified.

Optical spectra were obtained through multi-slit masks for 813 objects in the GSS between 1995 and 2001. The selection of objects is extensively discussed by Vogt *et al.* (2005), while the description of the reduction of spectroscopic data and redshift determination are found in Weiner *et al.* (2005). In summary, each mask was observed with a blue and red grating for a combined wavelength coverage of $\sim 5000 - 8200 \text{ \AA}$ depending on the slit placement on the mask. The spectral resolution is FWHM=2.9 \AA in the blue and 4.2 \AA in the red corresponding to 2 – 3 pixel sampling per resolution element. Typical exposure times were one hour per grating setup with fainter targets exposed for a few hours. Since most galaxies have sizes comparable to the seeing disk ($\sim 1''$), spectral information along the spatial direction is not available in most cases and a one-dimensional spectrum has been produced for each object by summing several pixels along the spatial axis. Six-hundred and twenty galaxy spectra were obtained in the survey and 576 have high enough signal-to-noise to yield redshifts with confidence levels of 90% and higher and allow measuring spectral line parameters (fluxes, widths and equivalent widths). For the purpose of identifying active galaxies, we measure several emission and absorption lines indicative of AGN activity. We considered only emission/absorption lines with signal-to-noise measurements greater than 5:1 in this paper.

The line measurements were performed using

two independent fitting techniques. The primary fitting algorithm was developed by one of the authors (A. C. P.) and employs a maximum likelihood estimation to perform an automated Gaussian fit to emission/absorption lines. The extracted sky spectrum was used to determine the noise at each position along the spectrum. For about 10% of the galaxies, however, the sky spectrum necessary for the error determination was not available in the DEEP database. For these objects we manually fit the line profiles using SPLOT in IRAF¹ as described in Kobulnicky *et al.* (2003). Each line was fit individually with a Gaussian profile except for the [OII] doublet, where two Gaussian profiles were fit simultaneously and the sum recorded. We empirically estimate the error in the line flux as $\sigma_L = \sqrt{12} \times \text{rms}$, where 12 is the number of pixels summed in a given emission line for this resolution, and rms is the root-mean-squared variations in an adjacent offline region of the spectrum. The equivalent width error is determined as

$$\sigma_{EW} = \sqrt{\frac{\sigma_L^2}{C^2} + \frac{L^2}{C^4} \sigma_C^2} \quad (1)$$

where L, C, σ_L , and σ_C are the line and continuum levels in photons and their associated 1σ uncertainties. The error in the continuum is determined by fitting the baseline regions around each line. We used both fitting techniques to measure a broad sample of emission and absorption lines from several galaxy spectra in order to compare the measured values and errors. The line flux, width, continuum values and errors were in general agreement to within 5%.

For equivalent width measurements, the determination of the continuum level is particularly important. In almost all cases, the continuum has been averaged over a large number of pixels in the wavelength direction, which allows this value to be well determined. The typical S/N in the continuum is well above 5 around the majority of emission/absorption lines for most sources. Those with the weakest continuum measurements (just under 1 count per 1500s of exposure time) have S/N of ~ 1.5 to 2.

¹IRAF is distributed by the National Optical Astronomy Observatories, which are operated by the Association of Universities for Research in Astronomy, Inc., under cooperative agreement with the National Science Foundation.

2.1. Spectroscopically Identified AGNs

2.1.1. Broad-Line AGNs

Active Galactic Nuclei can be detected in galaxy spectra through the presence of broad, permitted lines covering a wide range of ionization. The galaxy spectra in the GSS span a wide redshift range ($0.05 < z < 3.35$) and thus we do not have complete coverage of any one particular line for the entire set of spectra. Therefore, we have identified and measured several emission lines known to be broadened in Seyfert 1 nuclei or QSOs (i.e. broad-line AGNs or BLAGNs). These lines include the strongest Hydrogen Balmer lines ($H\alpha$ and $H\beta$), $MgII$ ($\lambda 2800\text{\AA}$) and CII ($\lambda 2326\text{\AA}$). We also measured $CIII$] ($\lambda 1909\text{\AA}$), CIV ($\lambda 1549\text{\AA}$) and $Ly\alpha$ ($\lambda 1215\text{\AA}$) for the higher redshift sources.

The definition of “broad” for BLAGNs is not well defined in the literature. The criterion in terms of FWHM ranges between 1000 and 2000 km/s (e.g. Weedman 1977, Steidel *et al.* 2002). Recently, Hao *et al.* (2005) found a bimodal distribution of $H\alpha$ FWHMs in a study of over 80,000 galaxy spectra from the Sloan Digital Sky Survey (SDSS). These results suggest that BLAGNs can be classified as those galaxies with $FWHM(H\alpha) > 1200$ km/s. For the sake of uniformity, we have applied this criterion to all possibly broadened emission lines in the spectral range of the GSS galaxies to identify BLAGNs. In fact, the measurements discussed here show little ambiguity in the identification of BLAGNs which display marked differences from their narrow-line counterparts.

Of the 576 GSS spectra, 563 have at least one of the necessary emission lines within the spectral range. $H\alpha$ is in the wavelength range for 129 galaxies and found in emission for 55 sources though none displays widths greater than 400 km/s. The $H\beta$ line is in emission in 226 out of 410 possible galaxy spectra. One galaxy, 283_3452, displays broadened $H\beta$ with a velocity of 4900 km/s. Only seven out of 201 spectra with $MgII$ in range display this rare emission line. Of these seven galaxies, six are broad with velocities between 4300 and 8300 km/s. Two of the six display considerable self-absorption of the broadened $MgII$ emission line preventing an accurate measurement of the velocity width (085_5273 and 152_6235). The $MgII$ emission in 152_6235 is particularly weak compared to the broad emis-

sion lines in the other galaxies. However, there is also evidence of $CIII$] at the blue edge of the spectrum which also appears slightly broad. This adds some confidence to the classification of this galaxy as a BLAGN, though we note that this classification is less certain than the others. One other galaxy with narrow $MgII$ emission, 092_3172, also displays $MgII$ absorption lines on either side of the emission line but the overall shape of the emission does not appear to be broad. Two of 48 galaxies with CII in range show the line in emission. One of these, 083_5407, is broadened and also contains broad $MgII$. None of the spectra contain CIV emission. Only three high redshift sources contain $Ly\alpha$ in their wavelength range. Two of these show the line in emission with widths less than 300 km/s. Thus, a total of 7 galaxies, one with broad $H\beta$, five with broad $MgII$ alone and one with $MgII$ and CII , display broadened emission lines meeting our criteria. These galaxies are listed in Table 1 in order of increasing redshift. The spectra and images of these objects are shown in the first 7 panels of Figures 1 and 2.

2.1.2. [NeV] and Broadened [OIII] as AGN Diagnostics

The presence of $[NeV](\lambda 3426\text{\AA})$ indicates an ionizing potential of at least 97.02 eV, too high to be produced through star-formation alone but possible through accretion onto a supermassive blackhole (e.g. Hall *et al.* 2000). We detect $[NeV]$ in only 3 of the 393 galaxies with this line within their spectral range (see Table 2 and Figures 1 and 2). The velocity widths of the $[NeV]$ line range from 390 to 650 km/s. One of these, 073_7749, shows additional Balmer absorption lines indicative of a post-starburst galaxy. The other two are also classified as BLAGNs based on broad $H\beta$ and $MgII$. Objects 292_3076 and 083_0815 also show weak $[NeV]$ emission, though it is below our signal-to-noise ratio for a significant detection.

Broadened $[OIII](\lambda 5007\text{\AA})$ is also an indicator of AGN activity. The analysis of SDSS spectra (Hao 2003; Zakamska *et al.* 2003) reveals that AGNs typically have $FWHM([OIII]) > 400$ km/s whereas widths for normal star-forming galaxies are much lower. The $[OIII]$ line is in the spectral range of 386 galaxies, being detected in 192. Only two (142_4838 and 292_3076) reveal broadened $[OIII]$ with velocities of 450 km/s and 820 km/s

respectively and are listed in Table 2 (spectra and images in Figures 1 and 2). Object 142_4838 is also a BLAGN.

2.1.3. Narrow-Line AGNs

A number of criteria have been used to identify narrow-line AGNs (NLAGNs), which can be differentiated from normal star-forming galaxies using the emission-line ratios of the most prominent optical lines such as [OII]($\lambda 3727\text{\AA}$), [OIII]($\lambda 4959, 5007\text{\AA}$), [NII]($\lambda 6583\text{\AA}$), [SII]($\lambda 6716, 6731\text{\AA}$), H α and H β (e.g. Veilleux & Osterbrock 1987). For a large fraction of galaxies in the GSS, however, many of these lines are redshifted out of the optical range. In addition, the GSS spectra are not flux calibrated, making it impossible to compare flux ratios for emission lines in different regions of the spectrum. For these reasons, most traditional line ratio diagnostics are not applicable to our survey data.²

A novel emission line diagnostic to identify NLAGNs proposed by Rola, Terlevich & Terlevich (1997; RTT) uses the equivalent widths of the [OII] and H β and allows classifying galaxies to $z \simeq 0.8$ without the need flux calibration. Two distinct zones define the AGN region of the diagram, at $\text{EW}(\text{H}\beta) < 10$ and $\text{EW}(\text{OII})/\text{EW}(\text{H}\beta) > 3.5$. Using a sample of local emission line galaxies, RTT find that 87% of the AGNs reside in these regions while 88% of the HII galaxies fall in the remaining region (see their Figure 3b). The AGN and HII samples are comprised of integrated galaxy spectra while the LINER spectra are extracted from the nuclear regions of the galaxies. Using $z \leq 0.3$ emission-line galaxies from the Canada-France Redshift Survey (Tresse *et al.* 1996), RTT find good agreement between their technique and classical diagnostic diagrams. The CFRS sample also contains spatially integrated spectra as DEEP1, though, with a much lower resolution. Although this technique does not perfectly separate the star-forming galaxies from AGNs, it does a fairly good job of identifying the majority of NLAGNs in a sample of emission line galaxies.

²Since H α and [NII]/[SII] are close in wavelength and thus are not significantly affected by the lack of flux calibration, we did investigate this line ratio diagnostic but found no convincing AGN candidates among those galaxies with these lines in their spectra.

Of the 576 galaxies in our spectroscopic survey, 318 contain [OII] and H β in their spectral range, but only 115 display both lines in emission with greater than 5σ signal-to-noise. In two cases, the continuum at H β was negative due to uncertainties in the sky subtraction, making it impossible to measure the galaxies' equivalent widths. With the removal of these sources, we plot the remaining 113 on the RTT diagram in Figure 3a with a uniform correction of 3\AA for underlying stellar absorption (Kennicutt *et al.* 1992, Tresse *et al.* 1996). This correction has the effect of moving objects toward the HII/star-forming (SF) galaxy region of the diagram. Based on the RTT criterion, 39 out of 113 galaxies (35%) fall in the AGN regions of the diagram. This represents only those galaxies where the 1σ errorbars remain within the AGN regions of the diagram.

As an additional check on the validity of the AGN criterion from RTT, we have analyzed a local sample of emission line galaxies from the Kitt Peak International Spectroscopic Survey (KISS) (Salzer *et al.* 2000; Gronwall *et al.* 2004) using the RTT equivalent width diagram. KISS is a large-area, objective prism survey of galaxies selected on the basis of strong H α emission. At redshifts less than $z=0.1$, 318 galaxies from the KISS sample have follow-up spectroscopic observations that include the [OII] and H β emission lines. Twenty-six of these local galaxies are classified as AGN/LINERs using classical line ratio diagnostic diagrams (see Gronwall *et al.* 2002). Figure 3b shows the KISS star-forming galaxies (blue asterisks) and AGN/LINERs (red triangles). We have added 3\AA for underlying stellar absorption as done for the GSS galaxies. We find that a threshold of $\text{EW}(\text{OII})/\text{EW}(\text{H}\beta) > 5$ (dashed line in Figures 3a and 3b) maximizes the differentiation of the AGNs and normal star-forming KISS galaxy populations. With this new threshold, galaxies in the upper 2 quadrants (AGN regions) yield a 44% probability of being an AGN while the lower-right quadrant (star-forming galaxies) yields a 1% chance of being an AGN. The lower-left quadrant is a mixture of AGNs and star-forming galaxies (13% AGN; 87% SF). It is unclear why there is such disagreement between the results of RTT and the KISS emission-line galaxy analysis using their diagram. However, we will use the more conservative estimate of NLAGNs based on the KISS

galaxy sample. Assuming our emission-line galaxies are like the KISS sample, the 7 GSS galaxies which lie above the $EW(OII)/EW(H\beta) > 5$ threshold in Figure 3b have a 44% chance of being NLAGNs. An additional 15 galaxies lie in the lower-left quadrant containing a mix of AGNs and star-forming galaxies. Table 3 lists the 7 “moderate probability” NLAGNs followed by the 15 lower probability NLAGN candidates. The galaxy images are shown in Figure 2.

2.1.4. Absorption Line Selected AGN Candidates

A possible indicator of AGN activity suggested by Becker *et al.* (1997) is the presence of strong MgII and/or FeII absorption. Hall *et al.* (2000) identified 15 absorption-line selected AGN candidates from $0.73 < z < 1.33$ among the CNOC2 spectra. However, they point out that MgII absorption lines of comparable strength have also been identified in starburst galaxies (e.g. Storchi-Bergmann *et al.* 1995) and thus such sources can only be classified as AGN candidates. Only one of their 15 was confirmed as a BLAGN through IR spectroscopy. Through visual inspection, we identify 14 galaxies with significant MgII and/or FeII absorption among the 200 GSS spectra with these absorption features in their spectral range. We list these galaxies in Table 4 but do not consider them strong AGN candidates since there is no further AGN evidence in any of the spectra.

2.2. Summary of Spectroscopic AGNs

Using a variety of selection techniques, we have identified active galaxies and AGN candidates among the 576 GSS galaxies with high quality spectroscopic data. We find 7 BLAGNs, three [NeV] detected AGNs (two are also BLAGNs) and two broadened-[OIII] detected AGN (one is also a BLAGN). Based on [OII] and $H\beta$ equivalent width measurements, we have also tried to identify those narrow-line galaxies that may harbor AGN. We find 7 galaxies with a moderate probability of being NLAGNs (44%) and 15 galaxies with a marginal chance of being NLAGNs (13% probability) which we hereafter identify as AGN candidates. This results in a total of 31 unique galaxies identified as AGN/AGN candidates. Those with the highest probability of being AGNs are the 16 galaxies identified through the presence of broad emission lines, the moderate probability AGNs

from the EW diagram, the [NeV] detected galaxies and the broad [OIII] galaxies.

3. THE VARIABILITY SURVEY

To identify possible AGNs via variability, we have analyzed two epochs of HST images for a portion of the GSS. The original GSS was observed in the spring of 1994 and consisted of 27 WFPC2 fields (numbers 4 through 6 and 8 through 31) imaged in V (F606W) and I (F814W) with total exposure times of 2800s in V for each field. An adjacent field, known as the Westphal field (GSS field number 7), was observed in the V band for 24,400s. In the spring of 2001, 18 of the GSS fields were reobserved in the V band with exposure times of 4200s. An additional 3 fields, including the Westphal field, were reobserved in spring of 2002 with exposure times of 4200s (7200s for the Westphal field). Thus, a total of 20 of the original 27 GSS fields plus the Westphal field have been analyzed for variability. For the remainder of the paper, we analyze the Westphal field separately due to the significant difference in exposure time.

3.1. Image Processing and Photometry

The original GSS images were combined and processed using standard techniques discussed in Simard *et al.* (1999; 2002). Unlike the images obtained in 1994, the second epoch of images for the 21 GSS fields were obtained in dither mode to allow for the construction of higher resolution, “drizzled” images. For each field, 6 exposures with sub-pixel shifts were drizzled together to produce $0.05''$ resolution images for the Wide Field CCDs using the STSDAS DITHER package in IRAF. We then block averaged these images in two-by-two pixel blocks to produce the same resolution as the first epoch images obtained in 1994 ($0.1''$ /pixel).

We adopted the object coordinate catalogs for the GSS described in Vogt *et al.* (2005). All galaxy CCD positions were visually inspected to ensure centering on the nucleus of the galaxy. In cases where the galaxy morphology was irregular, the position was centered on the brightest pixel near the approximate center of the galaxy. For each of the 21 fields reobserved in 2001/2002, we mapped the object positions from the epoch 1 fields onto the epoch 2 fields. Several of the epoch 2 fields were not well aligned with the original images,

having offsets of up to ~ 80 pixels. We used GEOMAP and GEOXYTRAN in IRAF to determine the offsets and apply the transformation to the epoch 1 catalogs. A final visual inspection of the epoch 2 images overlaid with object positions ensured that identical galaxy nuclei were identified in each epoch.³

Only galaxies in the Wide Field (WF) CCDs were included in our photometric survey. The Planetary Camera (PC) CCD images do not extend as deep as the WF CCDs due to the different pixel scale. Additionally, the small field-of-view (FOV) offers little contribution to the total sky areal coverage. The overlapping nature of the GSS fields allows for coverage of the PC FOV with one of the WF CCDs of an adjacent field in most cases. A total of 6604 galaxy nuclei were identified for the photometric survey in the 20 GSS fields and 529 in the deeper Westphal field.

Aperture photometry was performed using IRAF PHOT on the galaxies in each field and epoch. We chose an aperture radius of 1.5 pixels or $0.15''$ to maximize light from an unresolved nuclear component and minimize light from the underlying host galaxy. This is the approximately the measured FWHM of unresolved stars in the WFPC2 images. We used a magnitude zero-point of 22.91 as determined for V-band (F606W) HST images (WFPC2 SYNPHOT update, May 1997).

3.2. Charge Transfer Efficiency Losses And Photometric Errors

After performing aperture photometry, nuclear variability is determined from the magnitude difference of measurements for a source at both epochs. However, charge transfer efficiency losses which have occurred over the seven year interval produce a systematic offset that correlates with position on the CCD and magnitude. This is the well known CTE effect (Whitmore *et al.* 1999;

³As an additional check that misaligned apertures from the different epochs did not effect the photometric results, we later compared the magnitude difference from epoch 1 to epoch 2 vs. the concentration index for each source in our survey. The concentration index is the difference between magnitudes measured within $r=0.15''$ and $0.2''$ apertures. The effects of poor centering should be more enhanced for concentrated galaxies than diffuse galaxies. We found no trend in the amount of variability vs. galaxy concentration and therefore conclude that the aperture centering in both epochs is robust and not a significant source of error.

Biretta *et al.* 2001) which causes targets farther from the CCD readout amplifier to appear fainter than similar targets near the amplifier. Sarajedini, Gilliland & Kasm (2003; SGK) performed a similar analysis on images of the Hubble Deep Field separated by five years and discuss the role of CTE losses in more detail. This effect must be empirically quantified and removed from the data in order to identify varying nuclei with statistical accuracy.

We found that differences in the slope of the CTE relation between the CCDs were significant and could easily be determined for each of the three WF CCDs individually. We combined the data for the 20 GSS fields, separated into individual datasets for objects identified in WF CCD #2, WF CCD #3 and WF CCD #4. The Westphal field was fitted separately. We adopted a two-step approach to determine the CTE relationship with object position and magnitude. First, we fit a linear surface to the X and Y object positions and the magnitude differences using SURFIT in IRAF for each CCD. The slopes of the relationship with X and Y were found to be different for each of the 3 WF CCDs. The fits were used to correct the magnitude difference values for position-dependent systematic offsets. Secondly, we fit the dependence of the magnitude difference with nuclear magnitude. A 3rd order fit was required to properly model the dependence in all 3 WF CCDs. This correction was then applied to the data to correct for the magnitude-dependent systematic offsets. The overall corrections to magnitude difference range from 0.05 to 0.25 magnitudes with an average offset of 0.15 centering the distribution around zero.

3.3. Variable Nuclei Detected in the GSS

The points in Figure 4 show nuclear magnitude vs. CTE-corrected magnitude difference for galaxies in the 20 GSS fields (Fig. 4a) and the deeper Westphal field (Fig. 4b). The magnitude cut-off at the faint end ($V_{nuc}=27$ for the 20 GSS fields and $V_{nuc}=28$ for the Westphal field) was identified as the point where the galaxy number counts peak. Faintward of these limits, the number counts sharply decline. With these limits, our photometric survey consists of 4512 objects in the 20 GSS fields and 357 in the deeper Westphal field.

To identify significant variables, we determine

the expected photometric error for non-variable sources. Ignoring obvious outliers, we binned the data along the magnitude axis in 0.5 mag bins with larger bins at the bright end to include a greater number of points, and fit the distribution of magnitude differences with a Gaussian. Each bin was well fit with a Gaussian and the sigma width in each bin was determined. These values were then fit with a 7th order polynomial to produce a smoothly varying photometric error as a function of magnitude. The average magnitude difference (or photometric error) does not vary with magnitude at the bright end. We thus determined a lower limit to the photometric error at this end of the distribution. Brightward of $V_{nuc}=23.8$, the minimum 1σ limit for the photometric error was found to be 0.058 based on the average value of all probable non-varying sources brighter than this limit. In the deeper Westphal field, the minimum 1σ photometric error was found to be 0.046 for galaxies brighter than $V_{nuc}=24.3$.

The solid line in Figure 4 represents the 3.2σ threshold. We have chosen this criterion to identify galaxies which have undergone a significant nuclear flux change between the two epochs. This threshold was found to yield the most robust selection of variables by minimizing both the number of statistical outliers in the survey (only 0.14% in a normal distribution) and the number of objects falling just at/above the threshold. In the 20 GSS fields, 24 variable nuclei are detected (blue triangles) from the 4512 galaxies surveyed brighter than $V_{nuc}=27$. One of these, 283_1832, appears to be a supernova in the disk of the spiral galaxy 283_1831 (Sharon 2003) and falls beyond the y -axis limit of the figure at $\Delta\text{Mag}\simeq 4$. In the Westphal field, 3 variable nuclei (blue triangles) are detected among the 357 galaxies surveyed to $V_{nuc}=28$. Approximately 6.5 of the total number of variables are expected to be statistical outliers in a Gaussian distribution (see discussion of errors below). Table 5 lists the 26 variable galaxies (omitting the likely supernova) in order of decreasing nuclear apparent magnitude with columns as follows: (1) DEEP ID, (2) Redshift, (3) V_{nuc} internal to $r=1.5$ pixel aperture, (4) Magnitude difference between 1994 and 2001/2002, and (5) Significance of change obtained when normalized by the expected error. Images of the variable galaxies are shown in Figure 2.

A comparable variability study for the HDF-N (SGK) provides a good comparison to the current GSS variability survey. Sixteen galaxies were identified in the HDF-N displaying significant nuclear flux changes over a 5 year interval. Figure 4 of SGK, however, shows that the variability threshold for the HDF-N is ~ 5 times lower than that for the GSS fields. The significantly lower photometric errors for non-varying sources in the HDF-N results from the first and second epoch observations being obtained with the same pointing and roll angle, such that sources were located on the same CCD pixels in each epoch. The GSS fields suffered from large offsets and orientation differences between the two epochs. This resulted in less accurate removal of CTE loss effects for the GSS. In addition, the dithering pattern for the second epoch observations resulted in differences in the combining and processing of the individual images. The combination of these effects resulted in greater photometric noise for the GSS galaxy photometry when compared to the HDF-N.

As discussed in SGK, there are two distinct completeness issues that affect this type of variability survey. The first is related to the incomplete time sampling of the variable sources we wish to detect. Variability surveys usually image the survey field several times over many years (e.g. Trevese *et al.* 1994; Hawkins 2002). Depending on the quality of the data, these surveys have shown that virtually all known AGNs will be found to vary if observed periodically over several years. Our study is limited by the fact that we have only two epochs with which to determine variability and therefore sample just two points on the lightcurve of a varying source. Because of this, we will be incomplete in our census of AGNs since some varying sources will lie at magnitudes close to their original magnitude measured in the first epoch and would thus be undetected in our survey.

We estimate our incompleteness due to under-sampling of the lightcurve by using variability data for QSOs obtained over several years. Because long term variability surveys for low-luminosity AGNs have not yet been published, we use a sample of 42 PG quasars from Giveon *et al.* (1999) and randomly select points along the lightcurve separated by 6.5 years (the average time interval between the epoch 1 and epoch 2 GSS images). The Giveon *et al.* quasar lightcurves cover 7 years with

a typical sampling interval of 40 days. Assuming the photometric error we determined for the GSS (solid line in Fig. 4), we can estimate the probability that the Giveon QSOs would be detected in our survey. The average change in magnitude between two points on the QSO lightcurve separated by 6.5 years is ~ 0.2 mag and is consistent with the intrinsic variability amplitude of 0.14 mag reported in Giveon *et al.* (1999). We quantify the completeness by simulating photometric measurements of the Giveon QSOs assuming the photometric error of our survey at a given magnitude. We then find the percentage of QSOs that would be detected above the 3.2σ threshold as a function of magnitude. The completeness gets lower with increasing magnitude since the variability threshold increases at fainter magnitudes. The detection rate of QSOs ranges from $\sim 45\%$ at the bright end of the distribution to about 3% at the faint end ($V_{nuc}=27$). To find the average survey completeness, we weight the detection rate or completeness values by the number of galaxies in 0.5 mag bins. This yields a weighted detection rate of 16% for survey galaxies down to $V_{nuc}=27$. At a limiting magnitude of $V_{nuc}=26$, 29% of the QSOs would be detected. At $V_{nuc}=24$ and brighter, 45% of the QSOs would be detected. Thus, the incompleteness due to lightcurve sampling is a strong function of the survey's limiting magnitude. Relaxing our variability threshold to 2.5σ would increase these values by $\sim 6-7\%$ but introduces many more spurious variables as statistical outliers.

The second incompleteness issue results from the use of a fixed aperture to detect nuclear variability. We use a small, fixed aperture to minimize dilution of the AGN light from the underlying host galaxy to be more sensitive to AGNs varying within bright hosts. The aperture size matches the FWHM of an unresolved point source in the HST images ($0.15''$ in diameter). The fixed aperture will include the same amount of light from an unresolved source regardless of its redshift. However, the aperture will contain a larger fraction of the underlying, resolved galaxy for higher redshift objects than for low- z sources. Because of this, the dilution of the nuclear light by the galaxy increases as a function of redshift and, consequently, as a function of nuclear magnitude. This issue is discussed in more detail in SGK, where they determine that variability surveys with fixed aper-

ture photometry become less sensitive to variable nuclei at $V_{nuc}\simeq 26.5$ to 27.5 in HST WFPC2 images. What this essentially means is that regardless of the depth of the photometry in a WFPC2 field, only nuclei brighter than ~ 27 are being uniformly surveyed for variable AGNs. The fact that the photometry in the HDF-N field extended to $V_{nuc}=29.0$ while all of the variables were found to be brighter than $V_{nuc}=27.0$ is consistent with this effect. In the deeper Westphal field we again see that although photometry extends to $V_{nuc}=28.0$, the variables are all brighter than $V_{nuc}=27.0$ (Fig. 4b). Thus, we consider only those galaxy nuclei brighter than $V_{nuc}=27.0$ in all GSS fields (including the Westphal field) to be uniformly surveyed for nuclear variability. The total number of galaxies surveyed to $V_{nuc}=27.0$ in all GSS fields is 4672 (4512 in the 20 GSS fields and 160 in the Westphal field).

Since the distribution of magnitude differences between epochs is well fit with a Gaussian, we expect 0.14% of galaxies to fall outside of the 3.2σ threshold as statistical outliers. With a total of 4672 galaxies, this results in ~ 6.5 galaxies. If we correct for these outliers and the expected incompleteness, the fraction of variable nuclei in our survey to $V_{nuc}=27.0$ is $\sim 2.6\pm 0.6\%$ ($(26-6.5)/0.16/4672$). A recent study of the Hubble Ultra Deep Field identified $\sim 1\%$ of the galaxies to $V=28$ as variable over a 4 month time interval (Cohen *et al.* 2006). This lower percentage may result from the fact that larger apertures encompassing the entire galaxy's flux were used and thus may be less sensitive to nuclear variations. In addition, the shorter time baseline is likely to be less complete in identifying AGNs than longer, multi-year surveys (e.g. Webb & Malkan 2000).

4. COMPARISON OF THE SPECTROSCOPIC AND VARIABILITY SURVEYS

Both the spectroscopic and the variability surveys presented here have identified AGN candidates. Unfortunately, neither survey has 100% complete coverage of the GSS and the two surveys only partially overlap each other. Because the entire GSS was not reobserved in 2001/2002, and due to the large offsets between the epoch 1 and epoch 2 images for some of the repeated fields, not

all galaxies with DEEP spectroscopy are included in the variability survey. A total of 358 galaxies are in common between the 7133 galaxies in the variability survey and the 576 galaxies with high quality spectra. Figure 5 shows the 358 galaxies with both spectroscopic and variability data plotted on a diagram similar to Figure 4 with nuclear magnitude along the X-axis and magnitude change on the Y-axis. Spectroscopically identified AGN candidates from Tables 1 through 3 are indicated on the diagram as follows: BLAGN - blue filled circles; moderate probability NLAGN identified in the upper two quadrants of Figure 3b - red triangles; lower probability NLAGN identified in the lower-left quadrant of Figure 3b - red open triangles; [NeV] selected - purple asterisks; and broad [OIII] selected - green squares.

Most notable in Figure 5 is the fact that 3 of the 4 BLAGNs which fall within the bounds of the variability survey (blue filled circles) are identified as significant variables. The BLAGNs are also the brightest variables in our survey. One possible NLAGN candidate (red open triangle in Fig. 5b) appears as a variable. Furthermore, some of the high-probability NLAGNs (red triangles) are near the 3.2σ significance level in Figure 5a. BLAGNs are known to exhibit variability in their continua while NLAGNs primarily display flux variations within particular emission lines. Since the broad, V-band images used in our photometric survey are more sensitive to continuum flux changes, it is not surprising that we find greater overlap with the spectroscopic BLAGNs while most of the NLAGNs are not significant variables.

5. OPTICAL PROPERTIES OF AGNS IN THE GSS

Figures 6 and 7⁴ show the distribution of spectroscopically and variability detected AGNs, respectively, compared to all GSS galaxies in redshift, absolute magnitude, apparent magnitude, morphology and color. The magnitudes shown are integrated galaxy magnitudes based on the galaxy model fitting from Simard *et al.* (1999; 2002). For those galaxies without model fits, we used

⁴To simplify comparisons, we have omitted the Westphal field galaxies from Figure 7 due to the exposure time difference with the other GSS fields.

0.75'' radius aperture magnitudes. Since galaxies without model fits are typically fainter and smaller, these aperture magnitudes should adequately measure the total light from the galaxy. In Figure 6a, galaxy redshift vs. absolute magnitude ($H_o=70$, $q_o=0.5$) is shown for all GSS galaxies in the spectroscopic survey to $z=2$ (black points). High probability AGNs are indicated with red squares and AGN candidates with blue triangles. The 7 BLAGNs are further indicated with larger red squares. The AGNs cover the full range of redshifts for the GSS survey, with the mean redshift being slightly higher for the AGNs ($\langle z \rangle = 0.73$ compared to $\langle z \rangle = 0.66$ for the GSS galaxies). The BLAGNs have the highest average redshift ($\langle z \rangle = 1.1$) and also have a mean absolute magnitude more than three magnitudes brighter ($\langle M_V \rangle = -22.6$) than the general GSS sample ($\langle M_V \rangle = -19.3$). The mean luminosity of the NLAGNs is $\langle M_V \rangle = -19.8$. We expect galaxy nuclei hosting AGNs to be generally brighter than non-AGN galaxies since the active nucleus will contribute significant luminosity to the galaxy. It has also been found that the host galaxies of AGNs are typically brighter than normal galaxies (Ho *et al.* 1997).

Figure 7a is analogous to Figure 6a for variable nuclei galaxies. Here we plot all galaxies in the photometric survey for which spectroscopic data also exist (black points) such that redshifts are known and absolute magnitudes can be calculated. Significant variables are indicated with red squares. As shown in Figure 5a, 5 variables are also included in the spectroscopic survey. The three most luminous variables are the BLAGNs detected in our variability survey. The other 2 variables have absolute magnitudes of -19.0 and -17.3, fainter than the average GSS galaxy magnitude of $\langle M_V \rangle = -19.3$.

The thick solid lines in Figures 6b, c, and d are the apparent magnitude, V-I color, and bulge-to-total flux histograms (normalized) of all GSS galaxies in the spectroscopic survey. Figures 7b, c, and d display these same distributions for all GSS galaxies in the variability survey. The hatched/cross-hatched histograms overplotted in Figures 6b – 6d represent the spectroscopically detected AGN candidates (hatched region) and higher-probability AGNs (cross-hatched region). In Figures 7b – d, the hatched histograms are

variable galaxies with $>3.2\sigma$ significance and the cross-hatched histograms represent $>4\sigma$ variables. The AGN histograms have been arbitrarily multiplied by a factor of 5 in Figure 6 and 40 in Figure 7 for display purposes.

The spectroscopic AGNs have brighter apparent magnitudes ($\langle V \rangle = 22.0$) than typical GSS galaxies ($\langle V \rangle = 23.0$). Comparing Figures 6b and 7b, the apparent magnitude distribution of the galaxies in the photometric survey extends ~ 1.5 magnitudes deeper than the spectroscopic survey. In addition, the detected variable galaxies cover the full range of magnitudes for the photometric survey with a mean value only slightly brighter ($\langle V \rangle = 24.0$) than that of all GSS galaxies ($\langle V \rangle = 24.5$). The situation is different in the spectroscopic survey, where the AGNs are significantly brighter than the typical GSS galaxy. This highlights one of the strengths of the variability selection technique. Such surveys can extend deeper, with considerably less telescope time, and the identified AGN candidates are not biased towards the brightest galaxies but cover the full apparent magnitude range of the survey.

The colors of galaxies in the spectroscopic and variability surveys are similar (Figures 6c and 7c). Although the mean color of galaxies in the variability survey is bluer than the spectroscopic survey ($\langle V-I \rangle = 0.63$ compared to 0.79), both distributions peak around $V-I \sim 0.6$ and have a similar range. A KS-test shows that the color distributions of the variability and spectroscopically selected AGNs are not significantly different (67% significance level). The redder colors observed for some of the AGN/AGN candidates may be due to dust which has been observed to be significant in Seyfert galaxies (Malkan, Gorjian & Tam 1998). The bluest AGNs in both the spectroscopic and variability selected samples are the BLAGNs which have a mean $V-I$ color of 0.45.

The bulge-to-total measurements (B/T) in Figures 6d and 7d are from Simard *et al.* (1999; 2002). These histograms represent only the subset of galaxies in the spectroscopic and variability surveys that have 2-d model information. In both histograms, we have removed the BLAGNs that have unresolved morphologies (three in the spectroscopic survey and two in the photometric survey). Since the galaxy fitting algorithm did not include a point source component, the model fits

for these objects are erroneous. While the other AGN/AGN candidates appear to have good model fits, in some cases the bulge measurement may be enhanced by an unresolved AGN component in the galaxy light profile. At the current time, 3-component (disk+bulge+point source) modeling does not exist for the GSS galaxies, so that determining the relative flux of point sources among the selected AGN candidates is beyond the scope of this paper.

Interestingly, the morphologies of the AGN/AGN candidates are not significantly different from the parent population of galaxies in both the spectroscopic and variability surveys. A KS-test comparing the AGN and normal galaxy distributions confirms that they are not significantly different. In both surveys, the mean B/T for AGNs is similar to normal GSS galaxies. However, a comparison of Figures 6d and 7d reveals that galaxies and AGNs in the variability survey are slightly more bulge-dominated than the spectroscopic survey galaxies ($\langle B/T \rangle \simeq 0.37$ vs. 0.25). This is also evident from a visual inspection of the galaxy images in Figure 2. The galaxies and AGNs in the spectroscopic survey may favor more disk-dominated systems since these galaxies are likely to have the strongest emission lines and therefore have more easily identifiable redshifts.

Only two of the AGN/AGN candidates from the spectroscopic and variability selected samples, 292_3076 and 172_5049, are among the E/S0s identified in Im *et al.* (2002). Among these, 172_5049, a lower-probability NLAGN, is a spheroid with a particularly blue color (Im *et al.* 2001). Their analysis indicates this object to be a low-luminosity spheroidal with color contours revealing a bluer central region than typical E/S0s. This evidence supports the assertion that an AGN may reside in the center of this galaxy.

6. X-RAY PROPERTIES OF SPECTROSCOPIC AND VARIABLE AGNS

Active Galactic Nuclei have long been known as powerful X-ray sources. Recent deep X-ray surveys of the sky have revealed that much of the X-ray background is dominated by AGN activity. X-ray surveys for AGNs are not as hindered by some of the effects from which optical surveys suffer, such as obscuration due to dust and contamination

from bright host galaxies. About 60% of the GSS has been observed with the XMM-Newton and Chandra X-ray telescopes. GSS fields 4 through 18 were observed with XMM-Newton (PI: T. Miyaji) and fields 4 through 14 with Chandra ACIS-I (PI: K. Nandra). A summary of the XMM detected sources is given in Miyaji *et al.* (2004) and the Chandra detections are summarized in Nandra *et al.* (2005). A total of 31 XMM and Chandra detected sources are identified within $1.5''$ of an optical counterpart in the DEEP catalog. Thirteen are detected with both Chandra and XMM, 7 with XMM only and 11 with Chandra only. Some sources were detected in one survey and not the other due to 1) the slightly larger FOV of the XMM survey and 2) the deeper flux limit of the Chandra survey. Table 6 lists the X-ray sources in order of decreasing full-band X-ray flux with the following columns: (1) DEEP ID, (2) offset between the X-ray and optical position, (3) XMM ID from Miyaji *et al.*, (4) Chandra ID from Nandra *et al.*, (5) full-band (0.5–10keV) X-ray flux in units of 10^{14} ergs/cm²/s, (6) hardness ratio (calculated as $F_X(2-10)/F_X(0.5-2)$), and (7) full-band X-ray luminosity. For sources detected with both Chandra and XMM, the Chandra coordinates, X-ray flux and hardness ratios are given in the table.

Ten of the 31 X-ray sources with optical counterparts have high quality spectroscopic data in the DEEP GSS survey and four of these are BLAGNs. Two of the three remaining BLAGNs in Table 1 are not covered by the X-ray surveys. Thus 80% of the X-ray covered BLAGNs in the spectroscopic survey are X-ray detected. The one non-detected BLAGN is also the faintest optical BLAGN. Based on the X-ray to optical flux ratio of sources detected in deep Chandra surveys (e.g Barger *et al.* 2003b), the expected X-ray flux for an object with this optical magnitude (approximately $R \simeq 24$) ranges over 2 orders of magnitude with the faintest limit at $F_X(0.5-2) \simeq 10^{-16}$ ergs/cm²/s. Since this corresponds to the soft-band detection limit of the 200ks Chandra data for the GSS, it is possible that this source is too faint to be detected. Of the other X-ray sources with spectroscopic information, one is a [NeV] detected AGN (073_7749). None of the 14 EW ratio detected NLAGNs which fell within the X-ray FOV were X-ray detected. In total, 5 of the 10 X-ray sources (50%) in the GSS spectroscopic sur-

vey show some evidence of AGN activity based on their spectroscopic signatures. If we consider all spectroscopically selected AGNs in the X-ray FOV there are 25 galaxies, 5 of which are X-ray detected (20%). Considering only the highest probability AGNs (BLAGNs, moderate probability NLAGNs, [NeV] detected, and broad [OIII] AGNs) results in 11 galaxies of which 5 are X-ray detected (45%). The BLAGNs are the most luminous X-ray sources in the survey and are also among the softest X-ray emitters, consistent with the majority of type I, QSO-like AGNs. The [NeV] detected AGN is among the hardest X-ray sources in the GSS and is consistent with the classification of this object as highly obscured, type 2 AGN. Given its redshift and hardness ratio, we estimate an obscuring column density of $N_H = 1.5 \times 10^{23}$.

Some of the X-ray sources which were not observed in the DEEP1 survey or did not reveal AGN signatures in their optical spectra were followed up with near-IR spectroscopic observations summarized in Miyaji *et al.* (2004). Four of the five targeted galaxies did show evidence of broad H α emission in the near-IR (see Table 7). Since the signal-to-noise for these observations is much lower than the optical spectroscopic data analyzed in this paper, these results were not considered in the above statistics. However, including these 4 NIR observed galaxies as spectroscopically identified AGN raises the percentage of X-ray sources with AGN spectroscopic signatures from 50% to 75% (9/12; the total with AGN signatures becomes 5+4 and the total number of X-ray sources with either optical or NIR spectroscopic follow-up is then 12). Clearly, a more complete spectroscopic survey extending into the near-IR would shed considerable light on the AGN nature of faint X-ray sources.

The galaxies detected in the variability survey that fall within the FOV of the X-ray data are shown in Figure 8. Of the 31 X-ray sources with optical counterparts, 19 are in the variability survey (red triangles). Sixteen are above the flux completeness limits and 4 of these are variable (3 in the GSS fields and one in the Westphal field). Two of these 4 are also BLAGNs while the other 2 are not covered in the spectroscopic survey. Thus, we find that 25% (4 out of 16) of the X-ray sources in the variability survey are significant variables. If we consider the number of significant variables

that are also X-ray sources, we find that 27% (4 out of 15) of variables in the X-ray FOV are X-ray detected. All 4 of the variables are soft X-ray emitters which is consistent with the earlier assertion that the optical variables are more likely to be type 1 AGNs. They are also among the most luminous X-ray sources. About half of the variables that do not show X-ray emission are expected to have X-ray fluxes too faint for detection, based on typical X-ray to optical flux ratios. Another two, 072.2372 and 094.6133, are larger galaxies or clumpy objects whose optical light is probably an overestimate of the AGN light and thus may also be too faint to be detected in the X-ray survey. The remaining few may be spurious variables or could have lower X-ray to optical flux ratios like those of transition objects between AGN and quiescent galaxies (Barger *et al.* 2003b).

To check for faint X-ray emission that may be just below the sensitivity limits of the X-ray data, we have stacked the Chandra images at the location of spectroscopically and variability selected AGNs which do not individually appear as X-ray detections. Within $8'$ of the Chandra aimpoint, there are 11 non-X-ray detected variable sources. The stacked counts, using a $1.5''$ extraction radius, do not reveal a statistically significant detection (1.3σ). However, a marginally significant detection (2.9σ) was found when stacking the 14 non-X-ray detected spectroscopic AGN/AGN candidates. These galaxies all come from the [OII]/H β EW selected sources listed in Table 3 (2 from the moderate probability group and 12 from the lower probability group). The stacks were performed with the soft-band X-ray data (0.5–2 keV), where the Chandra sensitivity is the greatest. There was no significant detection using the hard-band data alone or the full-band data (0.5–10 keV). The marginal X-ray detection of the [OII]/H β EW selected galaxies provides some additional supporting evidence for the AGN nature of galaxies selected via this method. The lack of a detection among the stacked variable sources may be due to their likely higher redshifts and subsequent lower X-ray fluxes as discussed above. The variable sources used in the stack are generally about ~ 2 magnitudes fainter than the [OII]/H β EW selected galaxies.

7. DISCUSSION

We have selected AGN/AGN candidates using two independent selection techniques; spectroscopic selection based primarily on emission lines, and variability selection based on significant flux changes in galactic nuclei over a ~ 7 year interval. Ideally, one would construct a luminosity function (LF) for both AGN samples for comparison with one another as well as other similar surveys. However, LFs constructed from our datasets are likely to be highly uncertain for the following reasons: 1) we do not have accurate knowledge of the luminosity of the AGN component in our spectroscopically or variability selected galaxies, 2) we have incomplete/non-uniform redshift coverage for the spectroscopic detection of AGN, and 3) the variability survey incompleteness estimate is quite high (84–55%) due to poor photometric repeatability in the GSS WFPC2 images (§3.3). In the following paragraphs, we make estimates to account for these issues in order to broadly place our findings in context with published AGN LFs.

In the spectroscopic survey, we have selected AGN candidates among various subsets of galaxies in which particular emission line features could be measured. To estimate the total AGN fraction among GSS galaxies, we first define the sets of probable Type 1 and Type 2 AGNs. The Type 1 AGNs are easily defined as those displaying broad emission lines (Table 1). Two of the three [NeV] detected sources are also BLAGNs. The other galaxy spectrum does not show indications of any broad emission lines even though MgII is within the spectroscopic range. Therefore, we will consider the other [NeV] detected source as a NLAGN. One of the two broad [OIII] galaxies is also a BLAGN with broad MgII. The other, 292.3076, does not show any broad lines although H β is within the spectral range and appears as an absorption feature. We will consider this galaxy also as a NLAGN, although its exact nature is uncertain. Thus we include one [NeV] galaxy and one broadened-[OIII] galaxy in the NLAGN group along with those galaxies identified via [OII]/H β EW in Figure 3a.

We compare the spectroscopic and variability survey galaxy samples with the general GSS catalog presented in Vogt *et al.* (2005) containing 11,547 objects to identify any selection biases

among our samples and determine a characteristic limiting magnitude for AGN identification using both of our selection techniques. For comparison with Vogt *et al.*, who determined the survey completeness as a function of combined V_{606} and I_{814} magnitudes in $r=0.75''$ apertures, we define the magnitude $GAL = (V_{606} + I_{814})/2$. We investigate galaxy selection as a function of magnitude, color ($(V-I)$ using $r=0.5''$ apertures) and light profile concentration (based on the difference between $r=0.15''$ and $0.2''$ aperture photometry). The variability survey is 60 to 70% complete over the full range of galaxy colors to $GAL = 24$. The incompleteness is largely due to the fact that only 2/3rds of the GSS had second epoch data for the variability analysis. Between magnitudes of 24 and 25, the completeness drops to about 50% and becomes a function of concentration, with low-concentration sources (i.e. low-surface brightness sources) being less complete (34%) than high-concentration sources (60%). The spectroscopic survey is generally less complete than the variability survey and the completeness drops as a function of magnitude. Much of the incompleteness is due to the limited areal coverage of the DEEP1 spectroscopic survey. At magnitudes greater than 21, the survey is 42% complete and drops to 30% at 23rd magnitude. Between 23rd and 24th magnitude the spectroscopic survey includes just 13% of galaxies. The completeness is roughly constant as a function of color but is systematically lower for high-concentration sources (stellar-like morphologies). Therefore, we include a correction for the possibility of missed BLAGN due to this morphological bias (described below).

The total number of galaxies in which NLAGNs could be identified includes all spectra with either [OII] and $H\beta$, [OIII], or [NeV] lines in the spectral range, amounting to 526 of the available 576 galaxies with spectroscopic information. Using the [OII]/ $H\beta$ EW diagram probabilities detailed in §2.1.3, and including the [NeV] and [OIII] selected galaxies that do not also contain broad-lines, we estimate the total percentage of NLAGNs to be $1.4 \pm 0.5\%$ at $GAL \leq 24$, $2.3 \pm 0.9\%$ at $GAL \leq 23$ and $2.5 \pm 1.4\%$ at $GAL \leq 22$. The NLAGNs lie in the redshift range $0.14 < z < 0.87$ with an average redshift of $z \simeq 0.5$. The NLAGNs have integrated galaxy absolute magnitudes between -22 to -18 (rest-frame B-band determined

using $H_o=70$, $q_o=0.5$, and k-corrections assuming a power-law spectrum with $\alpha=-1.0$).

The fraction of BLAGNs in the spectroscopic survey can be estimated by first determining the number of galaxies in the survey in which broad emission lines could be observed to a given limiting magnitude. To better estimate the total number of BLAGNs, we correct for the fact that the spectroscopic survey is less complete for point-like sources. By determining the completeness of stellar-like objects vs. non-stellar objects in unity magnitude bins, and multiplying by the fraction of BLAGNs identified among stellar-like objects at each magnitude, we estimate that ~ 3 BLAGNs are missed to $GAL \leq 24$. Taking this into account, the percentage of BLAGNs among GSS galaxies is $1.9 \pm 0.6\%$ at $GAL \leq 24$, $2.5 \pm 0.9\%$ at $GAL \leq 23$ and $5 \pm 1.9\%$ at $GAL \leq 22$. The BLAGNs in our survey lie in the redshift range $0.65 < z < 1.3$ and have integrated galaxy magnitudes of $M_B \simeq -24$ to -20 .

In the variability survey, the completeness corrected fraction of galaxies containing significant variable nuclei was found to be 2.6% to $V_{nuc} = 27.0$. This nuclear magnitude limit translates roughly to $GAL = 26$. In order to compare with the spectroscopic survey, we compute the fraction of galaxies containing variable nuclei to the same galaxy limiting magnitudes. A galaxy magnitude limit of $GAL \leq 24$ imposes a V_{nuc} limit of ~ 25 . Recall that the completeness in detecting nuclear variability changes as a function of magnitude. At $V_{nuc} \leq 25$, the weighted completeness is 50%. Correcting for this incompleteness and statistical outliers, the percentage of galaxies containing nuclear variables is $4.5 \pm 1.4\%$. Following the same procedure, we find the fraction of variables galaxies to be $5.4 \pm 2.4\%$ for $GAL \leq 23$ and $8.3 \pm 4.9\%$ for $GAL \leq 22$. The fraction of variables in GSS galaxies is systematically greater than the fraction of BLAGNs by a few percent, though the small numbers and subsequent large errorbars on these percentages do not make them significantly so. If the variables are primarily Type 1 AGNs, as suggested by the overlap in their samples at the bright end of the distribution, this difference is likely due to the ability of the variability technique to probe lower AGN/host galaxy flux ratios. Thus, about half of the detected variables may contain AGNs too faint to be identified on the basis of emission lines alone. This may be due to the intrinsic faint-

ness of the AGN or significant obscuration. We do not have redshift information for the majority of variability detected AGNs. For those with redshifts, the magnitudes lie between $M_B \simeq -24$ to -17 . Making a crude estimate of the redshifts for the remaining variables (15 of the galaxies) based on V-I color and magnitude, the majority of variable nuclei galaxies without spectroscopic follow-up fall between $M_B \simeq -19$ to -17 . Since we find no spectroscopic BLAGNs fainter than $M_B \simeq -20$, we can conclude that indeed the variability selection technique is more sensitive to intrinsically fainter AGNs and that this is the primary explanation for the difference in the numbers of detected AGN.

Previous estimates of the fraction of Type 1 and Type 2 AGNs in the local universe reveal varying results. Huchra & Burg (1992; HB92) reported 1% of local galaxies in the CfA Redshift Survey as BLAGNs (Seyfert 1s) and another 1% as NLAGNs (Seyfert 2s). Maiolino & Rieke (1995) determined that at least 5% of RSA galaxies are AGNs with a ratio of Seyfert 1s to Seyfert 2s of 1:4. This higher fraction appears to be a result of probing fainter active nuclei within galaxies of similar magnitudes. Comparing the luminosity functions of Seyfert galaxies determined by HB92 to that of Ulvestad & Ho (2001; UH01) helps to make this clearer. Figure 2 of UH01 shows that their survey of Palomar Seyferts has a number density that is a factor of 5–10 higher than that of the CfA survey. Ho & Peng (2001) show that their median nuclear magnitude is almost 3 magnitudes fainter than that probed by HB92.

Our spectroscopic survey is not sensitive to intrinsically faint AGN within host galaxies and thus our results should be more comparable to those of HB92, where the spectra contain light from the entire galaxy and not just the nuclear region. It is somewhat unexpected, however, that we find no BLAGNs fainter than $M_B = -20$. The LF of HB92 shows a steady increase from $M_B = -22$ extending to $M_B = -18$. For a proper comparison with HB92, we must compare the fraction of galaxies containing BLAGNs in the same absolute magnitude range. From Figure 1b in HB92, we see that about 2/3rds of the Type 1 AGNs lie in the absolute magnitude range of our spectroscopic BLAGN sample ($M_B \simeq -22$ to -20) which constitutes $1.0 \pm 0.3\%$ of the CfA redshift survey galaxies to this absolute magnitude limit. Thus, we find a marginally sig-

nificant increase in the fraction of galaxies containing BLAGNs in this absolute magnitude range, rising from $1.0 \pm 0.3\%$ locally to $1.9 \pm 0.6\%$ at $z \simeq 1$.

The NLAGNs in our survey cover roughly the same absolute magnitude range as the HB92 Type 2 Seyferts and are therefore valid for comparison. We find little evidence for any increase in the number of galaxies containing NLAGNs (1% locally to $1.4 \pm 0.5\%$ at $\langle z \rangle \simeq 0.5$). The increasing fraction to higher redshifts is more significant considering a brighter magnitude limit for our spectroscopic survey (2.5% are NLAGNs among galaxies brighter than 22nd magnitude). Tresse *et al.* (1996) found an increase in the number of NLAGNs to $z=0.3$ in the CFRS, which consists of integrated galaxy spectra like the DEEP survey but with lower resolution. Using traditional line ratio diagnostics, they find that $\sim 8\%$ of galaxies are NLAGNs. Both the results of Tresse *et al.* and the present study are sensitive to the underlying stellar absorption from the host galaxy, particularly the $H\beta$ emission line measurement. Although both studies have made estimates to account for the $H\beta$ EW measurement, uncertainties in these estimates may explain why the Tresse *et al.* fraction of NLAGNs among galaxies at $z=0.3$ is greater than that found in the present study at a higher average redshift. The general result is that the fraction of NLAGNs among galaxies at intermediate redshifts ($z=0.3$ to 0.8) shows a moderate increase when compared with the local population. We can quantify the total AGN increase by comparing both the NLAGN and BLAGN samples to the total number identified in the CfA redshift survey. They find $2 \pm 0.3\%$ of all surveyed galaxies are AGN. The total fraction of spectroscopically detected AGN in our survey is $3.3 \pm 0.8\%$ which yields an increase of $1.3 \pm 0.9\%$.

8. SUMMARY

We have used two independent and complementary optical selection techniques, spectroscopic and variability identification, to probe the AGN population out to redshifts of $z \sim 1$ in the Groth-Westphal Survey Strip. AGN/AGN candidates have been identified among the 576 GSS galaxies with high quality spectroscopic data. Thirty-one galaxies have revealed AGN spectroscopic signatures with 9 classified as “high probability”

AGNs, 7 as “moderate probability” AGNs, and 15 as “lower probability” AGN candidates. Seven of these display broad emission lines (Type 1 AGNs). We also identify 26 variable nuclei galaxies within the GSS which have displayed significant flux changes ($>3.2\sigma$) over a 6 to 7 year time interval. The primary overlap of the two surveys is the set of BLAGNs, of which 80% appear as variable. Only a few NLAGNs approach the 3.2σ variability significance limit, indicating that variability primarily selects Type 1 BLAGNs.

The BLAGNs have an average redshift of $\langle z \rangle = 1.1$ while the other spectroscopic and variability selected AGNs (with spectroscopic data) have redshifts closer to the mean of the general GSS galaxy population ($\langle z \rangle = 0.7$). The mean luminosity of the spectroscopically selected BLAGNs is more than three magnitudes brighter ($\langle M_V \rangle = -22.6$) than the GSS galaxy average ($\langle M_V \rangle = -19.3$). The NLAGNs are only slightly more luminous ($\langle M_V \rangle = -19.8$) than the average GSS galaxy. The variability survey probes galaxies ~ 1.5 magnitudes fainter than the spectroscopic survey and the AGNs identified via variability are more representative of the entire magnitude range of galaxies. The identified AGNs in both surveys have colors and morphologies similar to their parent galaxy populations.

Eighty percent of the BLAGNs are detected in Chandra/XMM X-ray surveys and these are among the most X-ray luminous sources in the GSS. Only one of the high probability NLAGNs is X-ray detected: a [NeV] emission line galaxy with very hard X-ray emission. Of the variable nuclei galaxies within the X-ray FOV, 27% are X-ray detected. This can be compared to the HDF-N (SGK) where 44% of the variable nuclei galaxies were also X-ray sources. The higher percentage in the HDF-N is likely a result of better completeness of the variability survey and deeper X-ray observations of the field (2Ms compared to 200ks). The BLAGNs and variable nuclei are among the softest X-ray sources detected. A summary of all possible AGNs in the GSS identified via spectroscopy, variability or X-ray detection is given in Table 7. Along with the GSS ID and redshift if known, the table gives the spectroscopic AGN classification, variability in sigma units above the detection threshold and the full-band X-ray flux from either Chandra or XMM in units of 10^{14} ergs/cm²/s.

We find that $1.4 \pm 0.5\%$ of galaxies to $V_{gal}=24$ are NLAGNs while $1.9 \pm 0.6\%$ are BLAGNs. The fraction of galaxies containing variable nuclei to the same limiting magnitude is $4.5 \pm 1.4\%$. While it appears that variability primarily selects Type 1 AGNs (i.e. BLAGNs), the variability survey probes intrinsically fainter galaxies ($M_B \leq -17$) than does the spectroscopic survey. This is primarily due to the ability of the high-resolution HST photometry to probe flux changes in the central, unresolved regions of the survey galaxies while the spectroscopic survey relies on integrated galaxy spectra. The fraction of spectroscopically identified BLAGNs and NLAGNs at $z \sim 1$ reveals a marginally significant increase of $1.3 \pm 0.9\%$ when compared to the local population.

The results of these surveys, together with recent X-ray surveys, are helping to uncover the population of AGNs among galaxies to $z \geq 1$. It is clear that no one survey wavelength or technique is able to identify all AGNs in a given field and that a multiwavelength, multi-technique approach is the best way to identify and study the AGN population and its evolution with redshift. As additional multiwavelength survey data becomes available for the GSS and Extended Groth Strip region (e.g. deep VLA, GALEX, Spitzer), a more accurate census of the AGN population to $z \sim 1$ will emerge.

This paper is based on observations with the NASA/ESA Hubble Space Telescope, obtained at the Space Telescope Science Institute, which is operated by the Association of Universities for Research in Astronomy, Inc., under NASA contract NAS5-26555 and observations with the Keck telescope, made possible by the W. M. Keck Foundation and NASA. Funding for DEEP was provided by NSF grants AST 95-29098 and AST 00-71198. This work was also supported by the STScI grant AR-09218.04.

REFERENCES

- Becker, R. H., Gregg, M. D., Hook, I. M., McMaon, R. G., White, R. L., & Helfand, D. J. 1997, ApJ, 479, L93
- Barger, A. J., Cowie, L. L., Capak, P., Alexander, D. M., Bauer, F. E., Brandt, W. N., Garmire, G. P., & Hornschemeier, A. E. 2003a, ApJL,

- 584, 61
- Barger, A. J., Cowie, L. L., Capak, P., Alexander, D. M., Bauer, F. E., Fernandez, E., Brandt, W. N., Garmire, G. P., & Hornschemeier, A. E. 2003b, *AJ*, 126, 632
- Bershady, M. A., Trevese, D., & Kron, R. G. 1998, *ApJ*, 496, 103
- Biretta, J., Baggett, S., Riess, A., Schultz, A., Casertano, S., Gonzaga, S., Heyer, I., Koekemoer, A., Mack, J., McMaster, M. 2001, *BAAS*, 198, 402
- Boyle, B. J., Shanks, T., Croom, S. M., Smith, R. J., Miller, L., Loaring, N., Heymans, C. 2000, *MNRAS*, 317, 1014
- Cheng, F. Z., Danese, L., De Zotti, G., & Franchisini, A. 1985, *MNRAS*, 212, 857
- Cohen, S. H., Ryan, R. E., Straughn, A. N., Hathi, H. P., Windhorst, R. A., Koekemoer, A. M., Pirzkal, N., Xu, C., Mobasher, S., Malhotra, S., Strolger, L.-G., & Rhoads, J. E. 2006, *ApJ*, 639, 731
- Davis, M. *et al.* , 2003, *SPIE*, 4834, 161
- Faber, S. M. *et al.* , 2005, *SPIE*, 4841, 1657
- Giveon, U., Maoz, D., Kaspi, S., Netzer, H., & Smith, P. S. 1999, *MNRAS*, 306, 637
- Gronwall, C., Salzer, J. J., Sarajedini, V. L., Jangren, A., Chomiuk, L., Moody, J. W., Frattare, L. M., & Boroson, T. A. 2004, *AJ*, 127, 1943
- Gronwall, C., Sarajedini, V. L., & Salzer, J. J. 2002, in *AGN Surveys, Proceedings of IAU Colloquium 184, ASP Conf. Proc. Vol. 284*, eds. R.F. Green, E.Ye. Khackikian, & D.B. Sanders, p.43
- Groth, E. J., Kristian, J. A., Lynds, R., O'Neil, E. J., Balsano, R., Rhodes, J., & WFPC-1 IDT. 1994, *BAAS*, 26, 1403
- Hall, P. B. *et al.* , 2000, *AJ*, 120, 2220
- Hao, L. 2003, Ph.D. thesis, Princeton Univ.
- Hao, L. *et al.* , 2005, *AJ*, 129, 1783
- Hartwick, F. D. A. & Schade, D. 1990, *ARA&A*, 28, 437
- Hawkins, M. R. S. 1986, *MNRAS*, 219, 417
- Hawkins, M. R. S. 2002, *MNRAS*, 329, 76
- Ho, L.C., Filippenko, A. & Sargent, W.L.W. 1997, *ApJS*, 112, 315
- Ho, L. C. & Peng, C. Y. 2001, *ApJ*, 555, 662
- Hook, I. M., McMahon, R. G., Boyle, B. J., Irwin, M. J. 1994, *MNRAS*, 268, 305
- Huchra, J. & Burg, R. 1992, *ApJ*, 393, 90
- Im, M., Faber, S. M., Gebhardt, K., Koo, D. C., Phillips, A. C., Schiavon, R. P., Simard, L., & Willmer, C. N. A. 2001, *AJ*, 122, 750
- Im, M., Simard, L., Faber, S. M., Koo, D. C., Gebhardt, K., Willmer, C. N. A., Phillips, A. C., Illingworth, G., Vogt, N. P., & Sarajedini, V. L. 2002, 571, 136
- Kennicutt, R. C. 1992, *ApJS*, 79, 255
- Kobulnicky, H. A., *et al.* 2003, 599, 1006
- Koehler, T., Groote, D., Reimers, D., & Wisotzki L. 1997, *A&A*, 325, 502
- Koo, D. C., *et al.* 1996, *ApJ*, 469, 535
- Koo, D. C., Kron, R. G., & Cudworth, K. M. 1986, *PASP*, 98, 285
- Lilly, S. J., Hammer, F., LeFevre, O., & Cramp-ton, D. 1995, *ApJ*, 455, 75
- Londish, D., Boyle B. J., & Schade, D. J. 2000, *MNRAS*, 318, 411
- Maia, M. A. G., Machado, R. S., & Willmer, C. N. A. 2003, *AJ*, 126, 1750
- Maiolino, R. & Rieke, G. H. 1995, *ApJ*, 454, 95
- Malkan, M. A., Gorjian, V., & Tam, R. 1998, *ApJS*, 117, 25
- Miyaji, T., Sarajedini, V. L., Griffiths, R. E., Yamada, T., Schurch, M., Cristobal-Hornilos, D., Motohara, K. 2004, *AJ*, 127, 3180
- Nandra, K., Laird, E. S., Adelberger, K., Gardner, J. P., Mushotzky, R. F., Rhodes, J., Steidel, C. C., Teplitz, H. I., & Arnaud, K. A. 2005, *MNRAS*, 356, 568
- Oke, J. B., Cohen, J. G., Carr, M., Dingizian, A., Harris, F. H., Lucinio, R., Labrecque, S., Schaal, W. & Southard, S. 1994, *SPIE*, 2198, 178
- Peterson, B. M., Wanders, I., Bertram, R., Hunley, J. F., Pogge, R. W., & Wagner, R. M. 1998, *ApJ*, 501, 82
- Rola, C. S., Terlevich, E., & Terlevich, R. J. 1997, *MNRAS*, 289, 419 (RTT)
- Salzer, J. J., *et al.* 2000, *AJ*, 120, 80

- Sarajedini, V. L., Gilliland, R. L., & Kasm, C. 2003, *ApJ*, 599, 173 (SGK)
- Sharon, K. 2003, M.Sc. Thesis, Tel-Aviv University
- Steidel, C. C. & Sargent, W. L. W. 1989, *ApJL*, 343, 33
- Steidel, C. C., Hunt, M. P., Shapley, A. E., Adelberger, K. L., Pettini, M., Dickinson, M., & Giavalisco, M. 2002, *ApJ*, 576, 653
- Steidel, C. C., Adelberger, K. L., Shapley, A. E., Pettini, M., Dickinson, M., & Giavalisco, M. 2003, *ApJ*, 592, 728
- Storchi-Bergmann, R., Kinney, A. L., & Challis, P. 1995, *ApJS*, 98, 103
- Schirber, M. & Bullock, J. S. 2003, *ApJ*, 584, 110
- Simard, L., *et al.* 1999, *ApJ*, 519, 563
- Simard, L., *et al.* 2002, *ApJS*, 142, 1
- Tresse, L., Rola, C., Hammer, F., Sstasinska, G., LeFevre, O., Lilly, S. J., & Crampton, D. 1996, *MNRAS*, 281, 847
- Trevese, D., Kron, R. G., Majewski, S. R., Bershadsky, M. A., & Koo, D.C. 1994, *ApJ*, 433, 494
- Ulvestad, J. S. & Ho, L. C. 2001, *ApJ*, 558, 561
- Veilleux, S. & Osterbrock, D. E. 1987, *ApJS*, 63, 295
- Vogt, N. P., *et al.* 2005, *ApJS*, 159, 41
- Webb, W. & Malkan, M. 2000, *ApJ*, 540, 652
- Weedman, D. W. 1977, *ARA&A*, 15, 69
- Weiner, B. J., *et al.* 2005, *ApJ*, 620, 595
- Whitmore, B., Heyer, I., Casertano, S. 1999, *PASP*, 111, 1559
- Zakamska, N. L. *et al.* 2003, *AJ*, 126, 2125

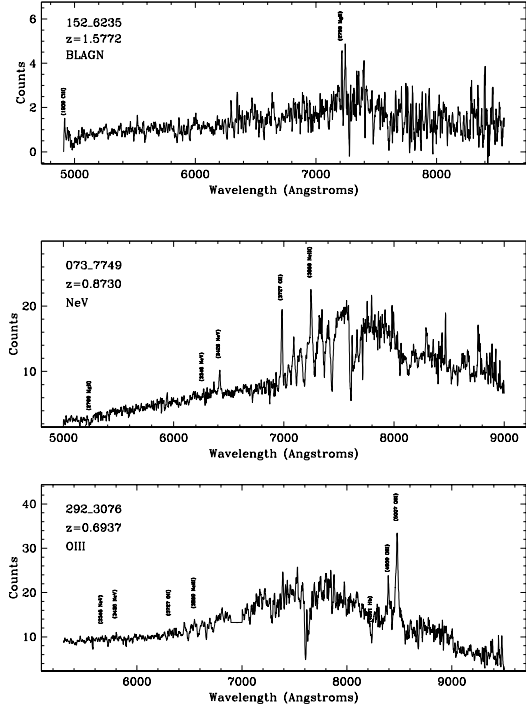
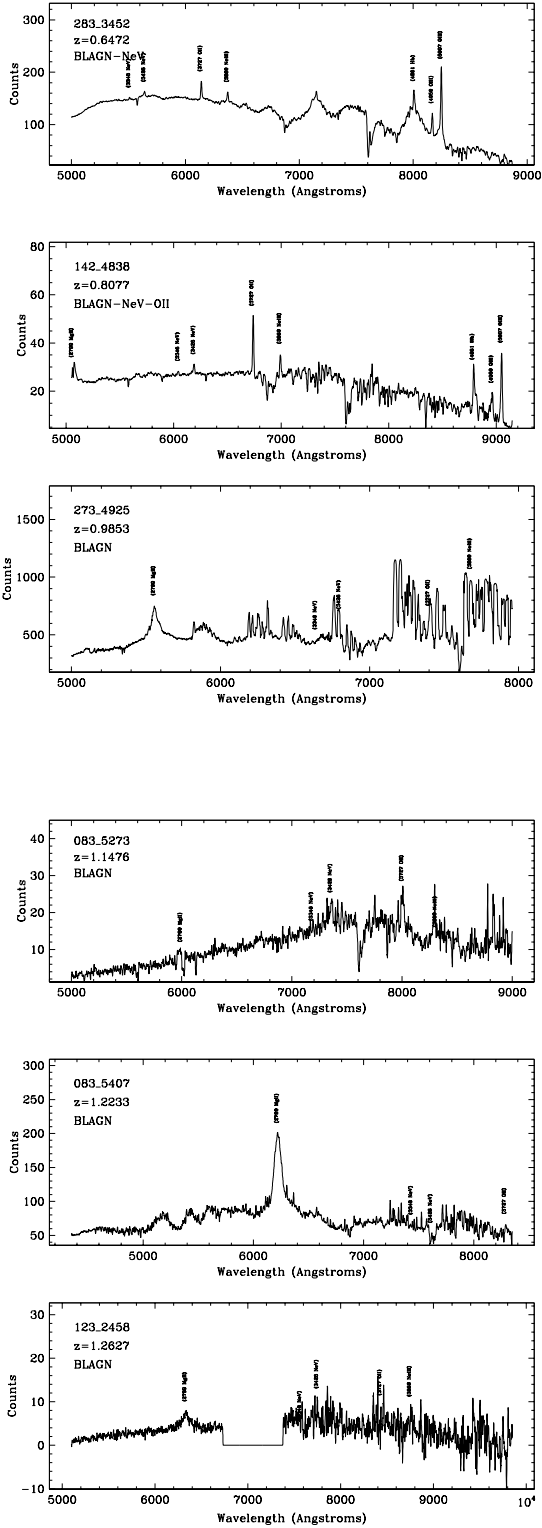


Fig. 1.— Galaxy spectra (smoothed by 7 pixels) for AGNs listed in Tables 1 and 2. Object 273_4925 was observed through a set-up star hole resulting in poor sky-subtraction. The gap in the spectrum of 123_2458 is a result of the non-overlapping wavelength range of the blue and red spectra for this object. The Y-axis is in units of ADU per pixel per 1500s exposure, where $\text{ADU} = e^-/2.4$.

Fig. 2.— See www.astro.ufl.edu/vicki/DEEP1-AGN for Figure 2. V-band Galaxy images for AGN/AGN candidates listed in Tables 1, 2, 3 and 5. Images labeled NLAGN are the 7 moderate probability NLAGNs from the upper quadrants of Figure 3. NLAGN-LO denotes those in the lower-left quadrant with a lower AGN probability. Images are $8'' \times 8''$. Additional image scales and wavelengths can be obtained at deep.ucolick.org.

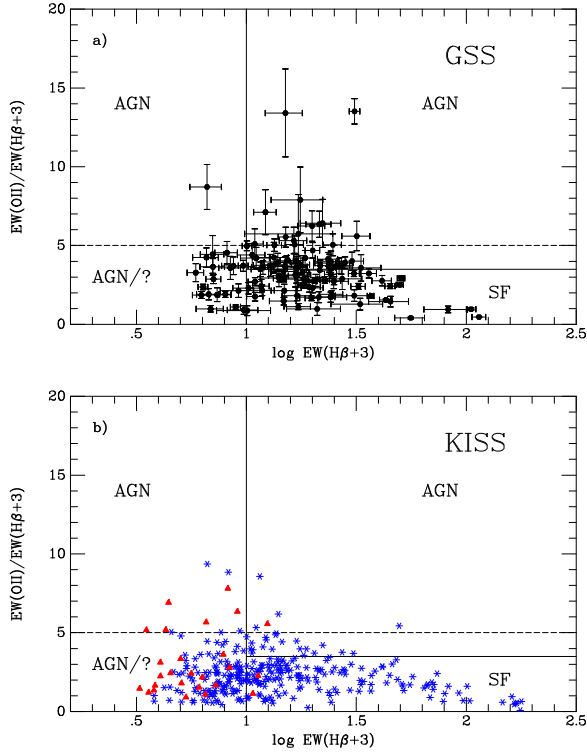


Fig. 3.— a) GSS galaxies (113) with measurable [OII] and $H\beta$ emission. Solid lines delineate AGNs from star-forming galaxy region according to Rola *et al.* (1997). 3\AA of absorption have been added to the $H\beta$ measurement. b) Local emission-line galaxies from the KISS survey (AGNs - red triangles; star-forming galaxies - blue asterisks) with 3\AA of absorption added to the $H\beta$ measurement. The dashed line best separates the KISS AGNs from the star-forming (SF) galaxies.

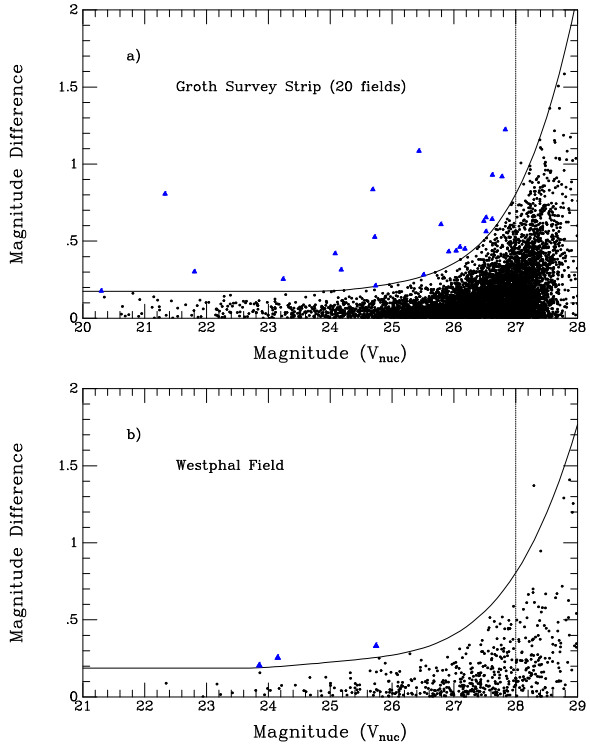


Fig. 4.— Absolute, CTE-corrected magnitude difference for objects in 20 Groth Strip Survey WFPC2 fields. The solid line is the 3.2σ limit indicating significant variables. Objects identified as candidate AGNs are indicated with blue triangles. b) Same as a) for the deeper exposure time Westphal field.

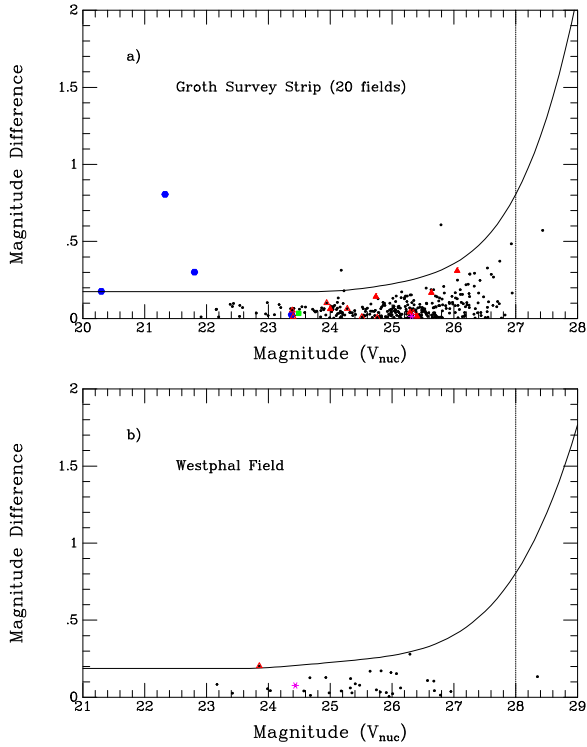


Fig. 5.— Same as Figure 4 but for sources covered in both the variability and spectroscopic survey. Spectroscopically identified AGN candidates are indicated as follows: BLAGN - blue circles, NLAGN (RTT diagram - moderate probability AGN) - red triangles, NLAGN (RTT diagram - lower probability AGN) - red open triangles, [NeV] selected - purple asterisks, broadened [OIII] - green squares.

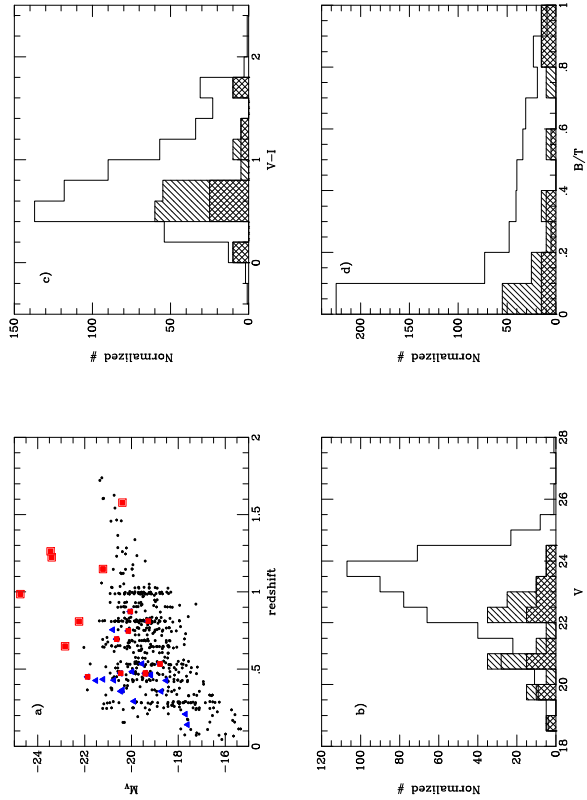


Fig. 6.— a) Redshift vs. absolute magnitude for GSS galaxies in the spectroscopic survey. Red squares indicate high and moderate probability AGNs and blue triangles are lower probability AGNs (see discussion in text). BLAGNs are further indicated with larger red squares. b) Histogram of V galaxy magnitudes for all GSS galaxies (thick solid line), all selected AGN/ AGN candidates (hatched region), and high and moderate probability AGNs (cross-hatched region). c) Histogram of V-I colors. d) Histogram of Bulge-to-Total flux ratios. AGN histograms are multiplied by a factor of 5 for display purposes.

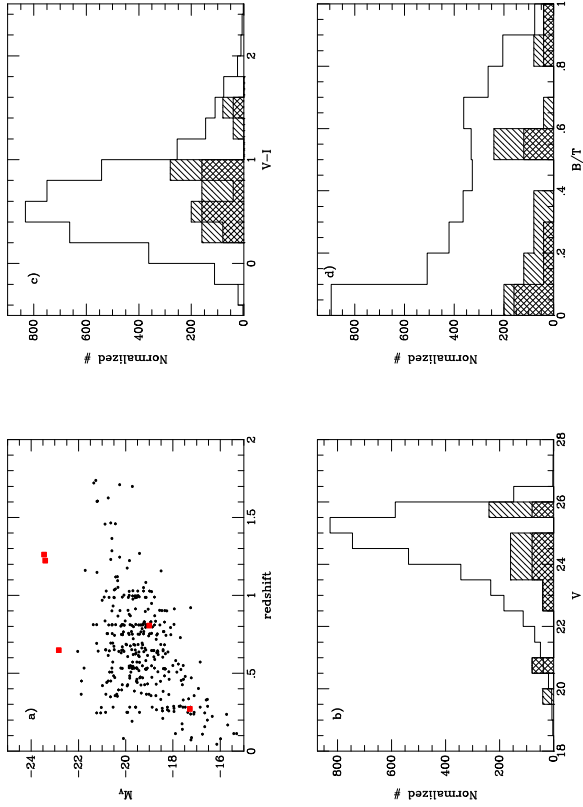


Fig. 7.— a) Redshift vs. absolute magnitude for GSS galaxies in the variability survey. Red squares are variable nuclei galaxies. b) Histogram of V galaxy magnitudes for all GSS galaxies (thick solid line), greater than 3.2σ variables (hatched region), and greater than 4σ variables (cross-hatched region). c) Histogram of V-I colors. d) Histogram of Bulge-to-Total flux ratios. AGN histograms are multiplied by 40 for display purposes.

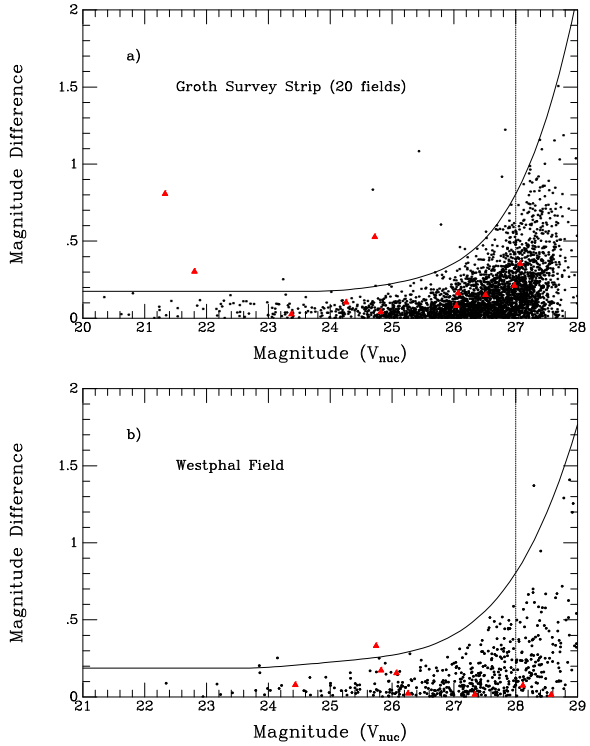


Fig. 8.— Same as Figure 4 but for sources covered in the Chandra and XMM X-ray surveys of the GSS. X-ray sources are indicated with red triangles.

TABLE 1
BROAD-LINE AGNS

DEEP ID	Redshift	Broad Line	V(km/s)	m_V	M_B
283_3452	0.6472	H β	4881	19.63	-22.51
142_4838	0.8077	MgII	...	20.75	-21.92
273_4925	0.9853	MgII	4322	18.73	-24.41
083_5273	1.1476	MgII	...	22.61	-20.90
083_5407	1.2233	MgII,CII	8330,8373	20.58	-23.08
123_2458	1.2627	MgII	4816	20.61	-23.13
152_6235	1.5772	MgII	...	24.21	-20.07

TABLE 2
[NeV] AND BROADENED [OIII] SELECTED AGNS

DEEP ID	Redshift	FWHM(km/s)	BLAGN?	m_V	M_B
[NeV]					
283_3452	0.6459	390	Yes	19.63	-22.51
142_4838	0.8065	540	Yes	20.75	-21.92
073_7749	0.8730	650	No	23.13	-19.72
Broadened [OIII]					
292_3076	0.6937	820	No	22.00	-20.31
142_4838	0.8065	452	Yes	20.75	-21.92

TABLE 3
 NLAGNs BASED ON [OII]/H β EW

DEEP ID	Redshift	[OII] EW	error	H β EW	error	m _V	M _B
284_4709	0.4498	57.71	1.25	3.62	1.08	19.75	-21.54
193_5426	0.4703	201.98	16.83	12.06	2.87	22.32	-19.08
223_6264	0.4715	87.03	14.07	9.23	1.44	21.27	-20.13
154_3015	0.4736	419.72	8.81	28.07	1.74	22.34	-19.07
133_2106	0.5328	124.27	7.91	16.93	2.80	23.23	-18.46
084_6809	0.7467	139.08	2.91	14.61	4.65	22.68	-19.80
084_4515	0.8108	136.35	1.53	18.46	2.79	23.72	-18.96
Lower probability NLAGNs							
083_1919	0.1406	19.32	2.90	2.88	0.51	21.37	-17.28
102_6577	0.2080	15.32	1.22	5.01	0.51	22.16	-17.37
072_4040	0.2908	31.22	7.45	4.03	0.86	20.72	-19.57
172_5049	0.3564	32.35	3.17	5.72	1.00	22.36	-18.39
173_5210	0.3570	37.06	3.83	5.15	0.95	20.63	-20.13
213_6640	0.3656	27.88	1.60	3.58	0.88	20.76	-20.05
072_2372	0.4258	9.79	1.12	5.93	0.47	22.98	-18.19
092_1962	0.4261	20.35	1.36	4.09	0.55	19.98	-21.19
113_0815	0.4279	6.78	1.00	3.88	0.98	20.76	-20.42
094_1054	0.4331	11.61	1.00	3.24	0.55	20.33	-20.87
103_1520	0.4620	15.09	0.81	3.35	0.33	22.50	-18.86
103_1811	0.4636	25.71	1.78	4.05	0.89	22.53	-18.83
072_7471	0.4830	30.25	5.18	5.45	0.95	21.82	-19.64
093_1519	0.5346	13.84	2.48	4.36	1.14	22.48	-19.22
084_4521	0.7540	12.82	1.85	3.74	0.81	22.04	-20.47

TABLE 4
 ABSORPTION-LINE SELECTED AGN CANDIDATES

DEEP ID	Redshift	Absorption Line
153_2622	0.8070	MgII
153_2422	0.8072	MgII
152_5051	0.8086	MgII
113_4933	0.8112	MgII
093_6661	0.9877	MgII/FeII
104_4809	0.9911	MgII
072_2928a	0.9972	FeII
092_3127	1.0510	MgII
064_6177	1.1449	MgII
083_0815	1.2849	MgII
212_2577	1.2859	MgII/FeII
223_7508	1.3658	FeII
084_1720	1.6058	MgII/FeII
113_6825	1.7217	MgII/FeII

TABLE 5
VARIABLE NUCLEI GALAXIES IN THE GSS

ID	Redshift	V_{nuc}	Δ_{nuc}	σ
283_3452	0.6472	20.299	0.176	3.24
083_5407	1.2233	21.330	0.806	14.83
123_2458	1.2627	21.806	0.301	5.54
054_2631	0.3780 ^a	23.238	0.253	4.65
253_3121	...	24.082	0.419	7.49
222_3954	0.2715	24.179	0.313	5.52
052_3372a	...	24.689	0.835	13.07
053_3424	1.5537 ^a	24.722	0.525	8.13
082_3939	1.1555 ^a	24.734	0.211	3.26
043_6232	...	25.436	1.084	13.12
263_6544	...	25.510	0.282	3.30
094_6133	0.8059	25.793	0.607	6.18
254_4642	...	25.915	0.431	4.09
284_2213	...	26.037	0.437	3.84
124_2138a	...	26.097	0.461	3.89
124_7332	...	26.179	0.450	3.59
274_6339	...	26.484	0.629	3.96
214_7315	...	26.518	0.653	4.00
124_4831	...	26.518	0.562	3.44
222_3930	...	26.617	0.642	3.61
272_6943	...	26.623	0.929	5.20
172_2078	...	26.778	0.918	4.48
042_4373	...	26.831	1.222	5.68
Westphal Field Variables				
072_2372	0.4258	23.854	0.203	3.42
074_5765	0.5989 ^a	24.149	0.253	4.11
074_6236	0.9346 ^a	25.742	0.329	4.11

^aPhotometric redshift derived from multi-color optical photometry (R. Brunner, private communications). All photo-z's are given in the DEEP database archive - deep.ucolick.org

TABLE 6
GSS X-RAY SOURCES WITH OPTICAL COUNTERPARTS

DEEP ID	offset	XMM ID	Chandra ID	F _{x14} ^a	Hardness Ratio ^b	log(L _x)
173-7369	0.50	x11	...	5.2	3.31	...
083-5273	0.62	x20	J141741.9+522823	5.0	2.92	44.25
142-4838	0.55	x10	J141651.2+522047	3.0	2.32	43.69
144-2774	0.34	x9	...	2.8	0.71	...
142-2752	1.23	x22	...	2.6	2.28	43.82 ^d
083-5407	0.45	x8	J141734.8+522810	2.1	2.06	43.94
062-2060	0.61	x52	J141745.9+523032	1.5	5.67	43.58
184-2148	1.29	x55	...	1.5	3.78	...
164-6109	1.15	x66	...	1.2	19.17	43.30
123-2458	0.21	x26	J141715.0+522312	1.0	2.00	43.65
082-5240	0.33	x44	J141729.9+522747	0.92	2.64	...
074-6236	1.21	x69	J141749.2+522811	0.90	3.59	43.37 ^d
053-4446	0.83	x61	J141758.9+523138	0.89	3.67	42.94 ^c
184-7960	1.16	x83	...	<0.86	soft	...
142-2530	0.46	x40	...	<0.67	soft	...
074-2638	1.23	x46	J141745.7+522801	0.61	2.59	42.41
053-3424	0.85	x125	J141756.8+523124	0.46	3.64	43.51 ^c
052-1037	1.07	x130	J141754.2+523123	0.32	1.70	42.87 ^c
073-7749	0.63	x146	J141745.4+522951	0.32	33.16	42.80
113-6354	0.03	x133	J141720.0+522500	0.31	4.57	42.58 ^c
053-1525	1.01	...	J141757.4+523106	0.19	4.39	43.77 ^e
064-2658	0.73	...	J141752.4+522853	0.17	hard	42.60 ^c
074-4426	1.27	...	J141747.0+522816	0.14	3.72	...
063-6344	0.77	...	J141751.7+523046	0.11	2.10	42.46 ^c
074-6044	0.62	...	J141749.2+522803	0.11	10.00	42.46
072-3963	0.64	...	J141737.3+522921	0.11	hard	42.18 ^c
063-4661	1.07	...	J141753.9+523033	0.11	3.42	42.46
082-3769	0.61	...	J141730.8+522818	0.099	hard	...
103-5524	0.42	...	J141723.6+522555	0.083	13.00	...
073-2249	0.43	...	J141746.7+522858	0.076	2.24	...
072-3223	0.64	...	J141739.0+522843	0.066	soft	...

^aFull-band X-ray flux for Chandra sources is from Table 3, column 7 in Nandra *et al.* (2005) and for XMM sources is from the summation of columns 5 and 6 of Table 2 in Miyaji *et al.* (2004).

^bA hardness ratio value of "hard" indicates the object was not detected in the soft (0.5–2 keV) X-ray band. Likewise, a value of "soft" indicates the object was not detected in the hard (2–10 keV) X-ray band. However, due to the greater instrument sensitivity in the soft band, a detection in this band alone does not necessarily indicate a particularly soft source.

^cX-ray luminosity calculated using photometric redshift or less certain spectroscopic redshift from DEEP database archive - deep.ucolick.org

^dX-ray luminosity calculated using redshift from Miyaji *et al.* (2004).

^egamma break galaxy - X-ray luminosity calculated using redshift from Steidel *et al.* (2003).

TABLE 7
SPECTROSCOPIC, VARIABLE AND X-RAY DETECTED AGNS

DEEP ID	Redshift	Spectroscopic Class	Variability (σ)	X-ray (F_{x14})
042_4373	5.68	0
043_6232	13.12	0
052_1037	0.9462 ^a	0.32
052_3372a	13.07	0
053_1525	3.0260 ^c	...	0.92	0.19
053_3424	1.5537 ^a	...	8.13	0.46
053_4446	0.6370 ^b	...	1.78	0.89
054_2631	0.3780 ^a	...	4.65	0
062_2060	0.9853	BLAGN-IR	...	1.5
063_4661	0.9976	none	...	0.11
063_6344	0.8929 ^a	0.11
064_2658	0.9515 ^a	0.17
072_2372	0.4258	NLAGN-LO	3.42	0
072_3223	0.23	0.066
072_3963	0.7421 ^a	...	0.10	0.11
072_4040	0.2908	NLAGN-LO	...	0
072_7471	0.4830	NLAGN-LO	...	0
073_2249	0.03	0.076
073_7749	0.8730	[NeV]	1.20	0.32
074_2638	0.4322	none	2.11	0.61
074_4426	0.26	0.14
074_6044	0.9966	none	1.77	0.11
074_6236	0.9950 ^d	BLAGN-IR	4.11	0.90
082_3769	0.85	0.099
082_3939	1.1555 ^a	...	3.26	0
082_5240	1.39	0.92
083_1919	0.1406	NLAGN-LO	0.22	0
083_5273	1.1476	BLAGN	0.46	5.0
083_5407	1.2233	BLAGN	14.83	2.1
084_4515	0.8108	NLAGN	0.16	0
084_4521	0.7540	NLAGN-LO	2.33	0
084_6809	0.7467	NLAGN	2.67	0
092_1962	0.4261	NLAGN-LO	...	0
093_1519	0.5346	NLAGN-LO	0.18	0
094_1054	0.4331	NLAGN-LO	...	0
094_6133	0.8059	none	6.18	0
102_6577	0.2080	NLAGN-LO	...	0
103_1520	0.4620	NLAGN-LO	...	0
103_1811	0.4636	NLAGN-LO	...	0
103_5524	0.083
113_0815	0.4279	NLAGN-LO	0.11	0

TABLE 7—*Continued*

DEEP ID	Redshift	Spectroscopic Class	Variability (σ)	X-ray (F_{x14})
113_6354	0.7037 ^a	...	0.95	0.31
123_2458	1.2627	BLAGN	5.54	1.0
124_2138a	3.89	0
124_4831	3.44	0
124_7332	3.59	0
133_2106	0.5328	NLAGN	0.50	0
142_2530	<0.67
142_2752	0.9830 ^d	BLAGN-IR	...	2.6
142_4838	0.8077	BLAGN,[NeV],[OIII]	...	3.0
144_2774	2.8
152_6235	1.5772	BLAGN	...	0
154_3015	0.4736	NLAGN	...	0
164_6109	0.8084	BLAGN-IR	...	1.2
172_2078	4.48	0
172_5049	0.3564	NLAGN-LO	0.98	0
173_5210	0.3570	NLAGN-LO	1.84	0
173_7369	5.2
184_2148	1.31	1.5
184_7960	<0.86
193_5426	0.4703	NLAGN	1.82	0
213_6640	0.3656	NLAGN-LO	1.11	...
214_7315	4.00	...
222_3930	3.61	...
222_3954	0.2715	none	5.52	...
223_6264	0.4715	NLAGN	2.16	...
253_3121	7.49	...
254_4642	4.09	...
263_6544	3.30	...
272_6943	5.20	...
273_4925	0.9853	BLAGN
274_6339	3.96	...
283_3452	0.6472	BLAGN,[NeV]	3.24	...
284_2213	3.84	...
284_4709	0.4498	NLAGN	1.10	...
292_3076	0.6937	[OIII]	0.61	...

^aPhotometric redshift

^bRedshift from CFRS (Lilly *et al.* 1995)

^cRedshift from Steidel *et al.* (2003)

^dRedshift from Miyaji *et al.* (2004)

NOTE.—If spectroscopic data exists but no AGN signature was identified, the spectroscopic class is “none”. A classification of NLAGN is a moderate probability NLAGN and a classification of NLAGN-LO is a lower probability NLAGN. BLAGN-IR indicates sources showing evidence of broad H α reported in Miyaji *et al.* (2004). If the object fell within either the Chandra or XMM FOV but was not detected, the X-ray flux is given as zero.